Robust signatures in the current–voltage characteristics of DNA molecules oriented between two graphene nanoribbon electrodes

2012 New J. Phys. 14 093049

(http://iopscience.iop.org/1367-2630/14/9/093049)

New Journal of Physics
The open-access journal for physics

Robust signatures in the current–voltage characteristics of DNA molecules oriented between two graphene nanoribbon electrodes

Carlos J Páez[1,2,5], **Peter A Schulz**[1,2], **Neil R Wilson**[3] **and Rudolf A Römer**[3,4,5]

[1] Instituto de Fisica Gleb Wataghin, Universidade Estadual de Campinas, Rua Sérgio Buarque de Holanda, 777 Cidade Universitária 13083-859 Campinas, SP, Brazil
[2] Faculdade de Ciências Aplicadas, Universidade Estadual de Campinas, 13484-350 Limeira, SP, Brazil
[3] Department of Physics, University of Warwick, Coventry CV4 7AL, UK
[4] Centre for Scientific Computing, University of Warwick, Coventry CV4 7AL, UK
E-mail: cjpaezg@ifi.unicamp.br and r.roemer@warwick.ac.uk

New Journal of Physics **14** (2012) 093049 (17pp)
Received 11 June 2012
Published 26 September 2012
Online at http://www.njp.org/
doi:10.1088/1367-2630/14/9/093049

Abstract. In this work, we numerically calculate the electric current through three kinds of DNA sequences (telomeric, λ-DNA and p53-DNA) described by different heuristic models. A bias voltage is applied between two zigzag edged graphene contacts attached to the DNA segments, while a gate terminal modulates the conductance of the molecule. Calculation of the current is performed by integrating the transmission function (calculated using the lattice Green's function) over the range of energies allowed by the chemical potentials. We show that a telomeric DNA sequence, when treated as a quantum wire in the fully coherent low-temperature regime, works as an excellent semiconductor. Clear steps are apparent in the current–voltage curves of telomeric sequences and are present independent of length and sequence initialization at the contacts. We also find that the molecule–electrode coupling can drastically influence the

[5] Authors to whom any correspondence should be addressed.

magnitude of the current. The difference between telomeric DNA and other DNAs, such as λ-DNA and DNA for the tumour suppressor p53, is particularly visible in the length dependence of the current.

Contents

1. Introduction

Following the publication of a seminal work by Fink and Schönenberger [1] on the electrical conduction of DNA strands and, shortly afterwards, a single molecule version by Porathet *et al* [2], the possibilities of electronic transport in DNA have so far stimulated a large body of work [3]. This is, of course, driven by the exciting fundamental characteristics of DNA as a biological structure with self-recognition and self-assembly properties. However, even after all this work, we are still far removed from a proper understanding of charge transport (CT) in DNA. Experimental work continues to remain very challenging and publications—while reporting tantalizing hints of surprisingly large currents—have only recently begun to probe CT properties in DNA beyond the magnitude of the supported current [4–6]. Similarly, the multitude of theoretical studies is yet to agree on which conduction mechanism and model to choose for a proper coarse-grained description of CT in DNA—or to find a means of attacking the complexities of larger DNA strands via powerful *ab initio* methods.

Part of the problem stems from the fact that DNA is not just a single molecule, but rather describes the whole set of DNA strands made possible by stringing the nucleotide bases adenine (A), cytosine (C), guanine (G) and thymine (T) into the classical double-helix structure. Consequently, it is difficult to compare the results of publications when the DNA sequences used are different or, as sometimes happens, not fully specified. Furthermore, the DNA sequences used range from simple periodic poly(dG)-poly(dC) variants—and of course

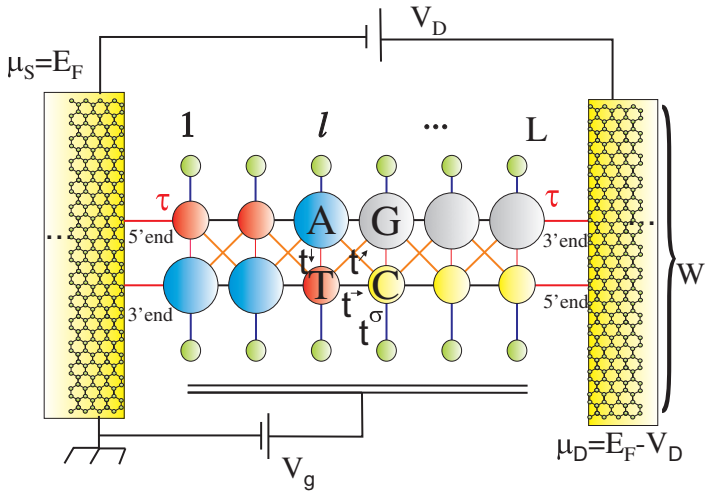

Figure 1. Schematic representation of a ladder-type model for electronic transport along DNA between two semi-infinite graphene nanoribbon source (S) and drain (D) contacts as indicated. A third (gate) terminal modulates the conductance of the molecule. The nucleotide base pair sequence is indicated by small (pyrimidines, red, yellow) and large (purines, blue and grey) circles, representing the four possible effective nucleotides, T, C, A and G, respectively. The sugar-phosphate backbone is given by green circles, and possible electronic pathways are shown by lines.

their AT counterparts—to viral, bacterial and eukaryotic DNA and beyond into artificially generated sequences.

Here, we intend to contribute to the discussion by putting forward a naturally occurring DNA sequence as a particularly well suited test bed for DNA experiments as well as theoretical studies: telomeric DNA. In mammals, it is a guanine-rich sequence in which the pattern TTAGGG is repeated over thousands of bases. Its length is known to vary widely between species and individuals and it essentially has a buffer function at the beginning and the end of DNA strands for eukaryote cells [7]. It therefore combines the advantages of a simple, periodic structure with the richness and biological function of a real DNA sequence. In addition, we shall study not a single, but rather five different coarse-grained, tight-binding models of DNA. In this way, and in the absence of a preferred model as discussed above, we shall not be over concerned with quantitative differences between the models, but rather aim to elucidate their qualitative agreement.

Some of the most exciting solutions to the well-established contact problem in nano-devices are based on the use of carbon allotropes such as carbon nanotubes (CNTs) [4, 5]. These CNTs then allow for good coupling to macroscopic gold contacts [8]. Even simpler should be the use of graphene flakes or nano-ribbons as a potential contact material [9, 10]; for example in [10], the advantage of such graphene contacts was attributed to their thermal stability, their versatility to anchor diverse molecules, particularly for π–π stacked aromatic rings, and the reduction in screening due to the enhanced gate coupling. Therefore, the basic building block of a DNA device might very well be a single graphene sheet into which gaps are fabricated by lithographic techniques. It is these devices which we will take as the starting point here (see figure 1).

2. Theoretical formulation

A schematic diagram of a molecule of DNA coupled to graphene electrodes is shown in figure 1. The source and drain electrodes are identified with their respective Fermi levels μ_S and μ_D; the effect is taken into account using self-energy functions [11]. A gate terminal modulates the conductance of the molecule. We focus on coherent transport and hence compute G^r, the retarded Green's function between the electrodes S and D, via the recursive lattice Green's function technique [12]. This then allows us to calculate the density of state, the transmission spectrum and the current–voltage characteristics.

2.1. The model Hamiltonians

The study of nanoelectronic applications based on macromolecules as the building blocks is a compromise between the model complexity and the length scale that the chosen model can handle. Therefore, the use of heuristic tight-binding models has attracted increasing interest over the last decade [13]. In spite of the simplified electronic structure, very long systems can be studied with these models in contradistinction to *ab initio* approaches. Hence, we study here the transport properties of DNA according to five such heuristic models. For the sake of clarity, the five models are briefly described as follows. First we address a single-strand chain with four different sites, representing the nucleotides (1L) [14]. This simplest possible model is followed by a single strand of bases attached to sites emulating the sugar-phosphate backbones (1L+BB or 'fishbone' model) [15]. Next in complexity appears a double-strand chain of nucleotides (2L) [16], and a model where the said double strand of base pairs is attached to backbones (2L+BB) [17] and, finally, a double strand of base pairs with backbones and additional diagonal inter-chain hoppings among base pairs (2L+BB+D) [18]. Before continuing, let us emphasize that our calculations are fully quantum coherent, i.e. we are interested in exploiting the use of DNA strands as nano-wires for potential nano-technological applications at $\sim$10 K or less, but not necessarily in the question of whether electronic CT plays a role at room temperatures [19] and other physiological conditions [3, 20]. For our quantum calculations, it is hence natural to restrict our investigations to DNA strands of length smaller than the persistence length (50 nm $\sim$150 bps) and we note that the contact distances used, e.g. in [21], were 8 nm ($\sim$23 bps) and DNA strands of length 10.4 nm had been employed.

Instead of repeating the mathematical definitions of the corresponding Hamiltonians as given in the above-cited literature, let us concentrate on the model 2L+BB+D as the most complicated one. The other four models can then be reconstructed from it by a suitable choice of parameters. In figure 1, we show a schematic representation of 2L+BB+D. The model contains parameters for the description of the backbone as well as longitudinal, transverse and diagonal base-to-base hopping terms which take into account the size difference between pyrimidines (C, T) and purines (A, G). The Hamiltonian can be written as

$$H_{\mathrm{DNA}} = \sum_{l=1}^{L} \Bigg[\sum_{\alpha=1}^{2} (\varepsilon_{l\alpha} |l,\alpha\rangle\langle l,\alpha| - t_{l,\alpha}^{\rightarrow} |l,\alpha\rangle\langle l+1,\alpha|) - t_l^{1\searrow 2} |l,1\rangle\langle l+1,2| - t_l^{2\nearrow 1} |l,2\rangle\langle l+1,1| - t_l^{\downarrow} |l,1\rangle\langle l,2| + \sum_{\sigma=\uparrow,\downarrow} (\varepsilon_l^{[\sigma]} |l,\sigma\rangle\langle l,\sigma| - t_l^{[\sigma]} |l,\alpha(\sigma)\rangle\langle l,\sigma|) \Bigg] + \mathrm{h.c.}, \tag{1}$$

where $t_{l,j}^{\rightarrow}$ is the hopping at base pair l along the strand starting from 5′ ($j = 1$) and 3′ ($j = 2$) ends, $t_l^{1\searrow 2}$ and $t_l^{2\nearrow 1}$ denote the diagonal hopping and $t_l^{\downarrow}$ is the hopping perpendicular from 5′ down to 3′ at l. The sum over σ in equation (1) marks the connection to the sugar-phosphate backbone as in figure 1. The Hermitian conjugate indicates the hopping terms associated with $t_{l,j}^{\leftarrow} = t_{l-1,j}^{\rightarrow}$, $t_l^{1\swarrow 2} = t_{l-1}^{2\nearrow 1}$, $t_l^{2\nwarrow 1} = t_{l-1}^{1\searrow 2}$, $t_l^{\uparrow} = t_l^{\downarrow}$ and $t_l^{[\sigma]}$. In addition, $\alpha(\sigma) = 1$ (2) for $\sigma = \uparrow$ ($\downarrow$) and $\epsilon_{l\alpha}$ and $\epsilon_l^{[\sigma]}$ denote the on-site energies on the two DNA strands and the top and bottom backbones, respectively.

The different terms are better appreciated by referring to figure 1. The on-site energies $\epsilon_{l\alpha}$ are taken to be the effective primary ionization energies of the base nucleotides, i.e. $\varepsilon_{\mathrm{A}} = 8.24\,\mathrm{eV}$, $\varepsilon_{\mathrm{T}} = 9.14\,\mathrm{eV}$, $\varepsilon_{\mathrm{C}} = 8.87\,\mathrm{eV}$ and $\varepsilon_{\mathrm{G}} = 7.75\,\mathrm{eV}$. In this work, we consider the backbone energy to be given as the average of the energies of the base nucleotides, i.e. $\varepsilon_l^{[\uparrow](\downarrow])} = 8.5\,\mathrm{eV}$ for all l. Both strands of DNA and the backbone are modelled explicitly and the different diagonal overlaps of the larger purines and the smaller pyrimidines are taken into account by suitable inter-strand couplings [18, 22]. The intra-strand couplings are $t_{l,\alpha}^{\rightarrow(\leftarrow)} = 0.35\,\mathrm{eV}$ between identical bases and 0.17 eV between different bases; the diagonal inter-strand couplings are $t_l^{1\swarrow 2} = t_{l-1}^{2\nearrow 1} = t_l^{2\nwarrow 1} = t_{l-1}^{1\searrow 2} = 0.1\,\mathrm{eV}$ for purine to purine, 0.01 eV for purine pyrimidine and 0.001 eV for pyrimidine to pyrimidine. Perpendicular couplings to the backbone sites are $t_l^{[\sigma]} = 0.7\,\mathrm{eV}$, and the perpendicular hopping across the hydrogen bond in a base pair is reduced to $t_l^{\downarrow} = 0.005\,\mathrm{eV}$. For previous discussions leading to these choices of parameters as well as the influence of the environment on the charge migration properties of the models, see the existing literature [17, 23–25]. Although we use rather simple Hamiltonians to describe the molecule, we believe that the qualitative physics of CT in the molecule is captured. This is because both the molecular energy levels and the wave functions closely resemble those calculated from the much more sophisticated *ab initio* theory [23]. Nevertheless, we emphasize that the choice of the tight-binding parameters is far from uniquely determined, being a rather controversial issue, and several parameter sets have been proposed in the literature [26].

2.2. Green's function techniques

The transmission probability $T(E)$ between the electrodes can be evaluated by

$$T(E) = \mathrm{Tr}\left[\Gamma_{\mathrm{S}} G^{\mathrm{r}} \Gamma_{\mathrm{D}} (G^{\mathrm{r}})^{\dagger}\right], \tag{2}$$

where G^{r} is the retarded Green's function of the system, which can be given as [11]

$$G^{\mathrm{r}} = [EI - H_{\mathrm{DNA}} - U - \Sigma_{\mathrm{S}} - \Sigma_{\mathrm{D}}]^{-1}. \tag{3}$$

Here I is the identity matrix, U is the gate potential and Σ_{S}, Σ_{D} are the self-energies for source (left) and drain (right) contacts (see figure 1), respectively. These self-energies are calculated as usual from g, the Green's function of the electrode [11], and the coupling τ between the DNA molecule and electrode (see figure 1), i.e. $\Sigma_{\mathrm{S,D}} = \tau_{\mathrm{S,D}}^{\dagger} g_{\mathrm{S,D}} \tau_{\mathrm{S,D}}$. The Green's functions G^{r} and g are calculated using a recursive technique [27]. The electrode–molecule coupling τ is determined by the geometry of the chemical bond [28]. We use a constant coupling $\tau = 0.35\,\mathrm{eV}$ of a similar magnitude as the inter-chain DNA couplings [2]. We emphasize that our results remain robust for small changes in this parameter. The anti-Hermitian part of the self-energy is known as the broadening function and related to the lifetimes $\Gamma_{\mathrm{S,D}} = \mathrm{i}(\Sigma_{\mathrm{S,D}} - \Sigma_{\mathrm{S,D}}^{\dagger})$ of an electron in a molecular eigenstate. The Hückel approach [29] predicts that the Fermi energy E_{F} is closer to the highest occupied molecular orbital (HOMO) level. In this work, the

Fermi energy of the Dirac cones in undoped graphene is aligned to the mid-gap (∼8.1 eV) of the DNA model shown in figure 1. Consequently, the Fermi levels in source and drain are $\mu_S = E_F$ and $\mu_D = E_F + eV_D$, respectively. The gate potential U, which allows us to model the charging effects in the presence of bias [30], can be expressed as $U = eV_g$ assuming that there is no large charge redistribution by applying bias between the electrodes.

Given H, $\Sigma_{S,D}$, the chemical potentials $\mu_{S,D}$ in the electrodes and the gate potential U, we obtain the density of states (DOS) from G^r as

$$\rho(E) = -\tfrac{1}{\pi}\mathrm{Tr}\{\mathrm{Im}[G^r(r, E)]\} \tag{4}$$

and the current is given as usual via $I = -\frac{2e}{h}\int_{-\infty}^{\infty} T(E)\,[f_S(E) - f_D(E)]\,\mathrm{d}E$. In the low-temperature limit such that $|e|V_D = \mu_S - \mu_D \gg k_B T$, we have $f_{S,D}(E) = \Theta(\mu_{S,D} - E)$, where Θ is the step function. So, the electronic low-T current can be expressed as [11]

$$I = -\frac{2e}{h}\int_{\mu_S}^{\mu_D} T(E)\,\mathrm{d}E. \tag{5}$$

3. Current–voltage characteristics along DNA systems

3.1. Selection of the DNA sequences

The results shown in figure 2 are the calculated I–V characteristics of three different types of DNA sequences for short DNA strands of length $L = 30$ bps. The sequences considered are (i) the eukaryotic telomere based on repeats of the TTAGGG sequence as we discussed in section 1 [7, 31], (ii) a random subsequence of bacteriophage λ-DNA [32, 33] and (iii) a random subsequence of the DNA strand of the p53 gene [34, 35]. The λ-DNA sequence has been studied previously as a typical example of a biological DNA sequence. It contains 48 502 base pairs with 25% of A, 24% of C, 28% of G and 23% of T strung together in a non-periodic sequence. Similarly, p53-DNA has 20 303 base pairs and is part of an important regulatory mechanism in humans [36–38].

3.2. Model dependence of the current–voltage characteristics

The main results for the I–V characteristics depicted in figure 2 can be summarized in a few general trends. First, the inclusion of backbones opens a gap between the HOMO and the lowest unoccupied molecular orbital, clearly revealed in the corresponding I–V curves showing threshold voltages [39]. Here it is worth recalling that we assume a Fermi energy close to half the energy gap, by tuning a gate voltage of $V_g = 9.8$ eV for all models (see appendix A). For sufficiently high applied voltages, the entire band will be scanned across the Fermi energy, leading to current saturation, as can be observed for almost all models for the voltage range depicted in figure 2 and further illustrated in the appendix. Next, a non-periodic sequence of base pairs, such as in λ- and p53-DNA, can drastically suppress the currents, even for such a short system of $L = 30$ bps, as one sees comparing figure 2, for disordered λ-DNA and p53-DNA, respectively, to the telomere sequence. This strong suppression is model dependent: single strands do not show a large suppression at such short lengths, while double-strand models already exhibit a six orders of magnitude drop in current. Furthermore, the double-stranded chain 2L+BB+D, i.e. with diagonal hopping and backbones, shows higher currents than the other double-stranded models, partially recovering single-strand values. Last, and important in

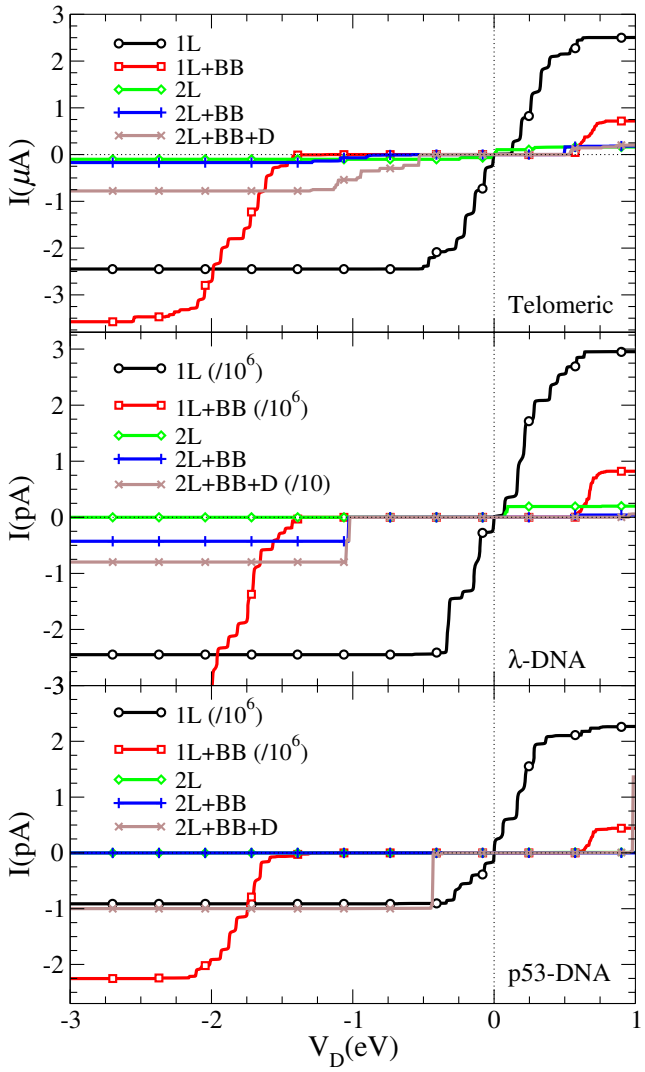

Figure 2. *I–V* characteristic for (top) telomeric, (centre) λ-DNA and (bottom) p53-DNA in five different heuristic models with $L = 30$ bps: (i) 1D, (ii) 1D with backbone (BB), (iii) and (iv) two channels without and with BB and (v) two channels with BB and diagonal coupling. Only every 100th symbol is shown for clarity. In the unidimensional case the hopping integrals $t_{i,i+1}$ are assumed to be nucleotide independent with $t_{i,i+1} = 0.4$ eV. The dotted horizontal and vertical lines indicate the $I = 0$ and $V = 0$ constants.

what follows, there are steps appearing in some *I–V* curves, which are due to resonances in the transmission probabilities. Such resonances are more relevant and robust in the telomeric sequences, due to the split of each band into several subbands [17]. Resonance effects are still present in some cases for disordered short sequences, but they do not last for longer systems, as can be systematically appreciated in figure 3. Hence we see that the DNA model proposed in equation (1) seems to interpolate between the extreme cases of the simple 1L models, retains the gap due to the backbone, but has smaller current values, which are more in line with the

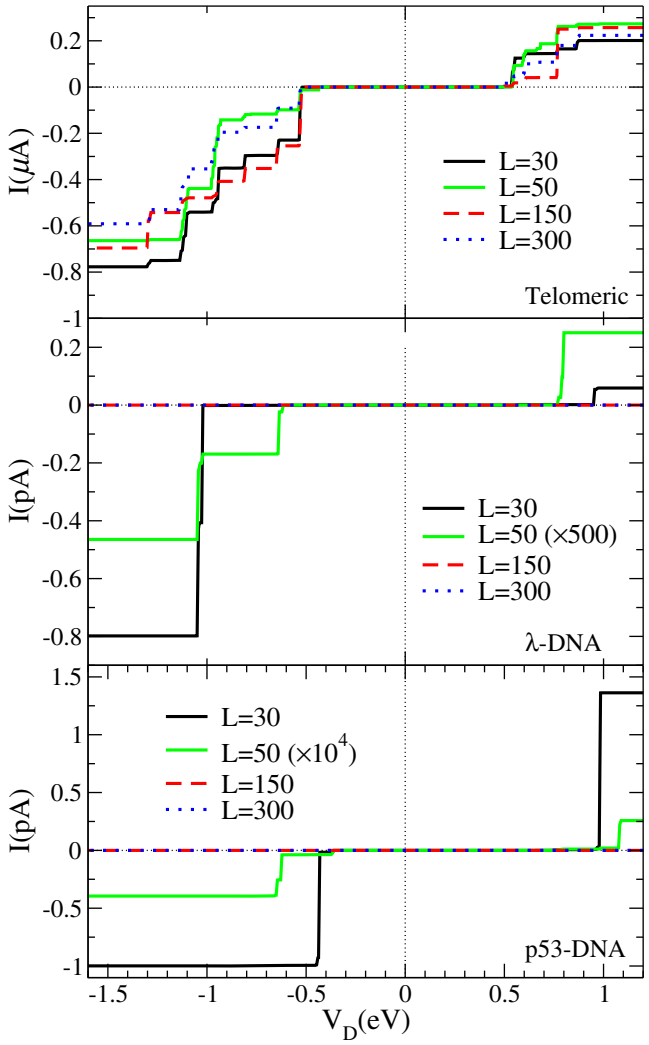

Figure 3. I–V characteristic of DNA segments with $L = 30$, 50, 150 and 300 bps for (top) telomeric, (centre) λ and (bottom) p53-DNA sequences. The thin dotted horizontal and vertical lines indicate the $I = 0$ and $V = 0$ constants.

experimental results. In what follows, all the results are for the model equation (1), namely 2L+BB+D, although it is the most complicated one of those considered previously.

3.3. Length dependence of the current–voltage characteristics

One of the most striking differences between the telomeric and the non-telomeric sequences is revealed by comparing short and longer sequences. Figure 3 shows the I–V characteristics for all three DNA strands, considering in each case four different strand lengths. The degree of non-periodicity in the sequences severely affects the I–V characteristics. First, there is the expected drop in the current due to non-periodicity (acting as an effective disorder), and the robustness of the step-like structures in the I–V curves for the telomeric strands at any L. Most prominent, however, is the rapid drop in the current with increasing L for the non-telomeric sequences. For 300 bps (104 nm), λ-DNA and p53-DNA, which are non-periodic, support practically no

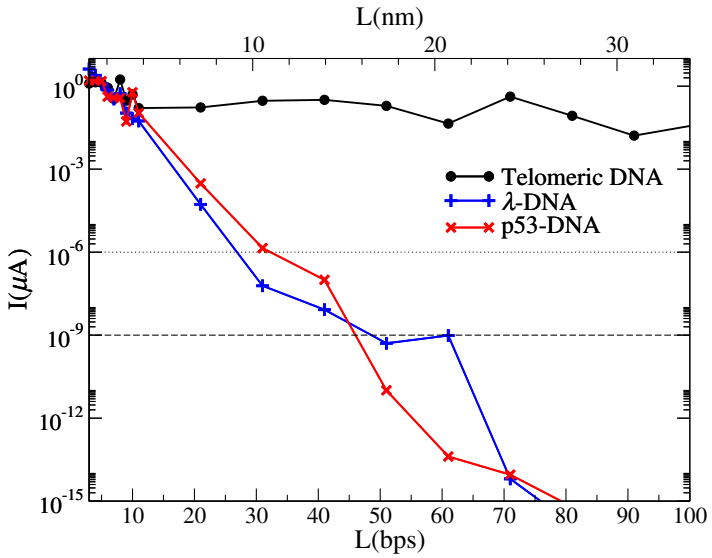

Figure 4. The current I as a function of length L for telomeric (•), λ-DNA (+) and p53-DNA (×) sequences at $V_D = 1.5$ eV. The thin horizontal dotted line corresponds to a current level of 10^{-12} A, which can be measured relatively easily, whereas the dashed line at 10^{-15} A indicates the limits of standard current measurement techniques.

current, even in the pA scale, while the telomeric sequence retains a maximum saturation current of around 0.6 μA.

Figure 4 shows the current of the three sequences as a function of length at a fixed saturation current $V_D = 1.5$ eV. For very short lengths up to $L \approx 10$ bps, the three cases cannot be distinguished. However, for longer strands, the telomeric sequence shows a saturation current of the order of several hundreds of nA almost constant in L, whereas for λ-DNA and p53-DNA the current decreases exponentially as the electronic states are strongly localized. It should be noted here that this result is robust and independent of the heuristic 2L+BB+D model, i.e. it happens in all the models considered. It should therefore be advantageous to consider the naturally occurring telomeres of DNA sequences as prime candidates when looking for good conductivity in a DNA strand—in nanotechnology applications but also in DNA-related *in vivo* processes where charge migration might be important [24].

4. Transport characteristics of telomeric DNA

In order to establish the features of the electronic transport which are intrinsic to the telomeric sequence, the role of the possible variations in coupling to the graphene contacts has to be studied. Three main aspects are considered: (i) the dependence on which base pair of the telomeric sequence is connected to the graphene, (ii) whether contacts are only made to a single strand of the DNA or to both, 3′ and 5′, ends and (iii) what happens when more than a single telomere is contacted in parallel. Let us recall that for the results presented up to now, we always assumed that the transport starts at the T of the TTAGGG sequence, that the coupling τ holds for both 3′ and 5′ ends and that only a single telomere has been contacted.

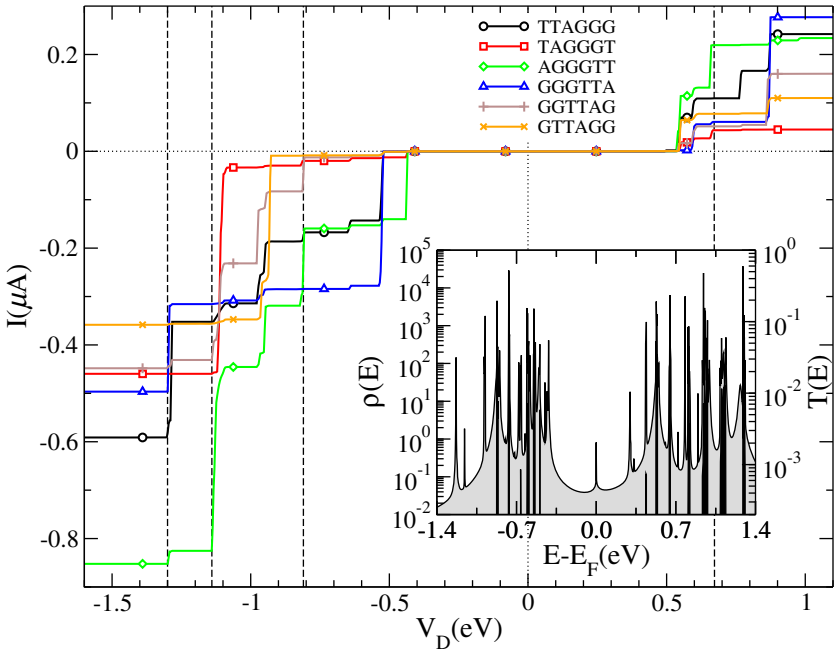

Figure 5. *I–V* characteristic for telomeric sequences ($L = 300$ bps long) and differently attached to the contacts. The inset shows how the sequence starts at the left contact in each case, with the first letter connected to the graphene edge. The dashed vertical lines mark, for example, four positions of very robust steps (see text). $I = 0$ and $V = 0$ constants are also indicated as in figure 4. Only every 100th data point is shown for clarity. Inset: DOS (grey shaded black line) and $T(E)$ (black line) for the telomere TTAGGG attached to the graphene contacts.

4.1. Starting the telomere

In figure 5, we show *I–V* curves for telomeric sequences starting at different base pair positions, i.e. in addition to the periodic repeat of TTAGGG, we also have TAGGGT, AGGGTT, ..., GTTAGG. In this way, we hope to capture the possibilities that might arise when the contacts are made simply by putting telomeres on top of graphene sheets[6]. The DOS of the TTAGGG system, as well as $T(E)$, is also shown in figure 5. The results are for $L = 300$ bps in all cases. The DOS shows a peak at E_F related to the nanoribbon localized state at this energy. The overall envelope of the DOS is shaped by the graphene band structure and the band splitting of the DNA system. The superposed sharp peaks are related to the resonances in $T(E)$, which show a large variation in intensity. Therefore, some peaks in the DOS are related to transmission peaks that fall below the scale of the figure. The irregular step-like structure in the *I–V* characteristics reflects the fragmented structure of $T(E)$. Note that the apparent gap in the *I–V* characteristics does not necessarily correspond to the gap in the DOS. The reason is that many of the states close to the band gap have very low transmission probabilities (related to highly localized resonances at different parts of the rather long sequences); therefore they do not contribute to transport.

When inspecting the *I–V* characteristics for the different starting positions, one notes that each one shows steps at the *same* energy, although the steps show variable amplitudes. We

[6] More sophisticated, wet-chemical methods can, of course, be used to ensure contacts at selected bases only [4, 5, 40].

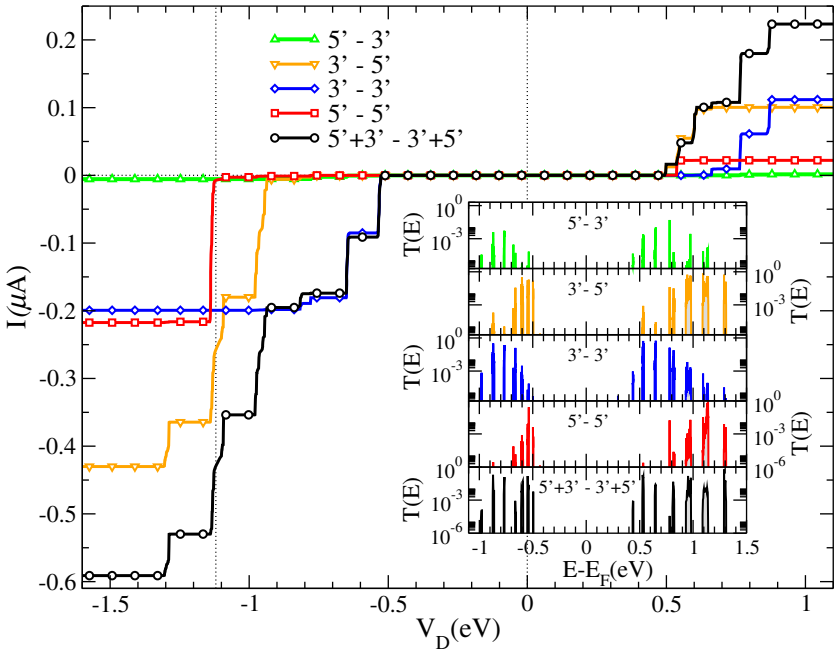

Figure 6. *I–V* characteristics for the finite DNA ladder, 300 bps long, contacted to electrodes in five different ways (see figure 1): source 5′ to drain 3′ (green △), source 3′ to drain 5′ (orange ▽), source 3′ to drain 3′ (blue ◇), source 5′ to drain 5′ (red □) and, lastly both source 5′ and 3′ to the drain 3′ and 5′ (black ○). The vertical dotted line denotes a robust step in the *I–V* curves for all contact geometries. $I = 0$ and $V = 0$ constants are also indicated as in the previous figures. Inset: $T(E)$ for five different contact situations with the same colours as in the main figure.

therefore find that, while changing the start of the sequence at the contact can alter the height of the transmission probability for a given energy, it does not change the position of the steps in the *I–V* curves. As we had argued in section 3, it is exactly the existence of these pronounced steps which makes the telomeric sequence stand out from other DNA sequences. Our result of the section now shows that this finding remains robust with respect to what actual base pair is chosen to contact to the graphene sheets.

4.2. Contacting the telomere at 3′, 5′ or both

In the literature [4, 5], it is known that the choice of contacting single 3′ and 5′ ends only or both 3′ and 5′ ends can alter the current response. This is also observed in our 2L+BB+D model—the class of 1L models, of course, cannot capture this behaviour—as we show in figure 6. In the figure, we have contacted the graphene electrodes via (i) only the direct 3′-to-5′ or 5′-to-3′ ends at source and drain, (ii) only the cross 3′-to-3′ or 5′-to-5′ ends and (iii) both 3′ and 5′ ends. Besides the trivial effect of dropping the current by reducing the number of channels, as readily observed by comparing the black curve to the others, one also sees that all cases show a significant modification of the subband transmission intensities in the energy range of interest around the Fermi energy. We interpret the difference between the 5′ and 3′ results in figure 6

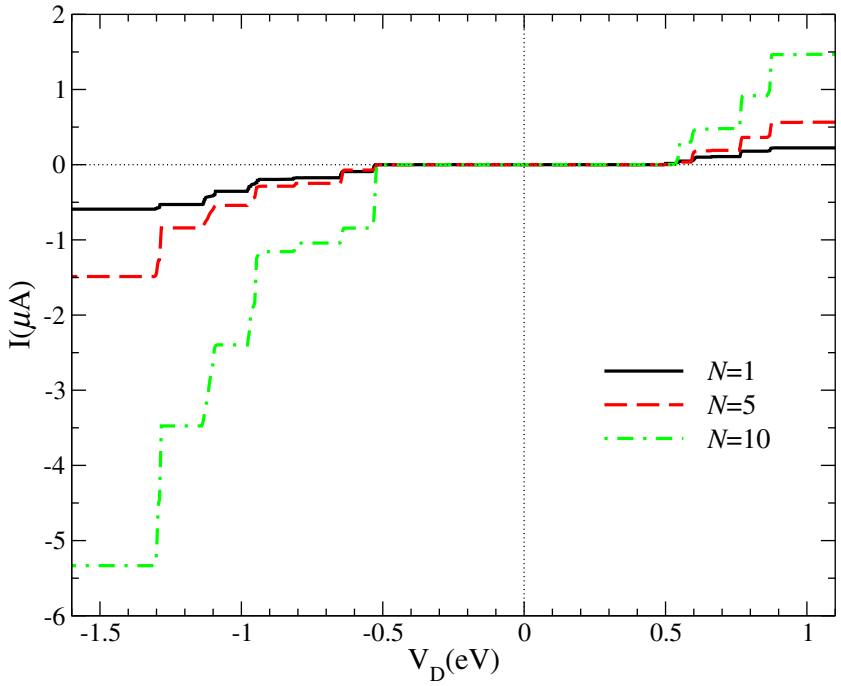

Figure 7. *I–V* characteristic for telomeric DNA arranged as $N = 1$, 5 and 10 parallel strands, each of which is 301 bps long.

as being due to the sequence of nitrogenous bases. In the source 5′ terminal, the on-site energy for the thymines (9.14 eV) is larger than the on-site energy for the adenine (8.24 eV) in the 3′ terminal. So, a contact via the A in 3′ is preferable. In addition, direct transmission as in 3′-to-5′ can make use of the larger hopping strengths compared to the diagonal or perpendicular couplings. We note, however, that this does not fully explain the sequence of current strengths, e.g. it is not immediately clear why the source 5′ to drain 5′ current is larger than the source 5′ to drain 3′ current. Nevertheless, the present results strongly suggest that the step structure of the *I–V* characteristics, although intrinsic to the telomeric sequence DOS, are filtered and selected by the choice of how the strands are coupled to the contacts. Note that we still observe that the (voltage) position of the steps remains fairly robust.

4.3. More than a single telomere in parallel

The advantage of the DNA device outlined in section 1 and shown in figure 1 is the macroscopic size of the graphene contacts together with a small, nano-sized gap to be manufactured into the graphene sheet. It is then clear that it will be hard to guarantee that only a single DNA strand lies across the gap. Hence, we expect that one might occasionally encounter a situation where more than one DNA strand is being contacted. As we shall show here, this seems indeed beneficial, i.e. we find that the situation of telomeric DNA strands contacted in parallel enhances the size of the current.

In figure 7, we show the *I–V* characteristics for a single sequence, together with the curves for five and ten sequences in parallel, all of them $L = 301$ bps long, and separated each by 40 C–C distances on the graphene contacts. We start the first sequence with TTAGGG... and

hence end after 301 bps as ...TTAGGGT. Then we use the remainder of the telomere as the start sequence of the next strand, i.e. TAGGGT...AGGGTT. The end of the fifth strand is then ...GTTAGG and the tenth strand ends as ...GGGTTA. In this way, we have different starting and end parts of the telomere at the source and drain contacts, respectively, for parallel sequences. From figure 5, we can see that the step structure is indeed enhanced and not washed out by adding many strands even if their assembly in an actual experiment is not base pair exact. It should also be noted that the currents are not a simple linear addition of the $N = 1$ case, since interference effects appear, due to the different sequences being coupled to the same contacts. Also, the position of the steps between plateaus remains again very robust.

5. Conclusions

The complexity of the DNA systems does not allow as yet a definitive conclusion to be drawn on the mechanism(s) leading to CT in telomeric or other sequences. Nevertheless, the consistency among the results found here for different heuristic models, widely discussed in the literature, suggests that important qualitative physical and chemical aspects have been captured in the present approach. Telomeric sequences contacted to graphene sheets may show high currents as well as robust plateau structures in the I–V characteristics. This plateau structure is enhanced and not washed out by adding parallel telomeric chains, irrespective of the starting points defined at the interface of each sequence with the contact. Most importantly, the drastic difference in the lengths dependence of the current for telomeric DNA as compared to other DNA strands such as the λ- and p53-DNA shown in figure 4 will allow for better comparison and interpretation of experimental data. We emphasize that the inclusion of some external disorder, be it in the fidelity of the sequence or the environmental conditions, does not drastically alter these differences [17]. An important current rectification behaviour can also be seen due to the differences in the transmission probabilities of occupied and unoccupied levels. A device including a gate electrode could further tune the rectification possibilities addressed here.

The devices investigated in this work—based on the naturally occurring, physiochemically stable telomeres—should provide ideal benchmark situations for systematic investigations of DNA electronic transport, as well as for the development of DNA-based molecular nanoelectronic applications using graphene as contacts. In particular, the I–V characteristics presented here show promise of a wide range of interesting nanocircuitry on complex patterns of hollowed graphene sheets bridged by telomeric DNA sequences.

Acknowledgments

CJP acknowledges financial support from FAPESP (Brazil) and the hospitality of the Centre for Scientific Computing at the University of Warwick (UK) where most of this work was developed. PAS acknowledges partial support from the CNPq (Brazil). NRW acknowledges support from the Warwick Centre for Analytical Science (EP/F034210/1).

Appendix A. Varying the gate voltage

Some features in the I–V characteristics depend on the gate voltage, V_g, applied to the system and are worth briefly discussing here. The gate voltage will shift the DOS modifying drastically

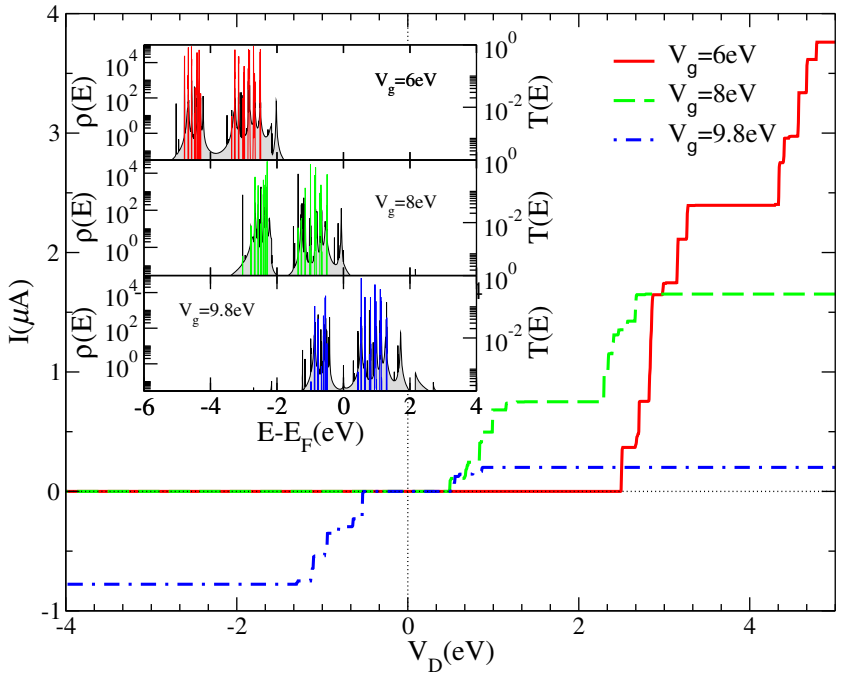

Figure A.1. *I–V* characteristics for telomeric DNA using ideal gate control ($\beta = 1$), $L = 30$ bps and three different V_g : $V_g = 6$ eV (red), $V_g = 8$ eV (green) and $V_g = 9.8$ eV (blue). Inset: density of states ρ (grey shaded) and transmission probability $T(E)$ (the same colours as in the main panel) for different gate voltages.

the transport characteristics. Keeping in mind that the main results shown in this paper are for $V_g = 9.8$ eV (bottom panel of figure A.1 inset, showing the transmission probability bands superposed on the density of states) a situation where the equilibrium Fermi energy lies closer to the HOMO (top of the valence band in semiconductor terminology), one observes that negative V_D show higher currents than positive V_g in figure A.1. This asymmetry is due to the lower transmission probability for the occupied molecular orbitals as compared to the unoccupied molecular orbitals. One can also appreciate how the saturation currents in the *I–V* characteristics are related to the energy ranges beyond the transmission bands. Diminishing the gate voltage, as in the examples shown in figure A.1 inset: $V_g = 8$ eV (centre panel) and $V_g = 6$ eV (top panel), it is possible to reach a situation of no current for negative V_D, as can be seen for the corresponding *I–V* characteristics in figure A.1.

Appendix B. Modelling the graphene contacts

The contacts to the DNA devices are semi-infinite graphene nanoribbons as depicted in figure 1. Graphene is a single layer of carbon atoms packed in a honeycomb lattice, composed of two sublattices. Finite pieces of graphene are limited by two different kinds of edges (or, more generally, a mixing of both kinds): armchair-like edges, where the atoms at the edges alternately belong to both sublattices and a zigzag edge, in which all the edge atoms belong to the same sublattice. The graphene contacts considered here are semi-infinite nanoribbons along the zigzag

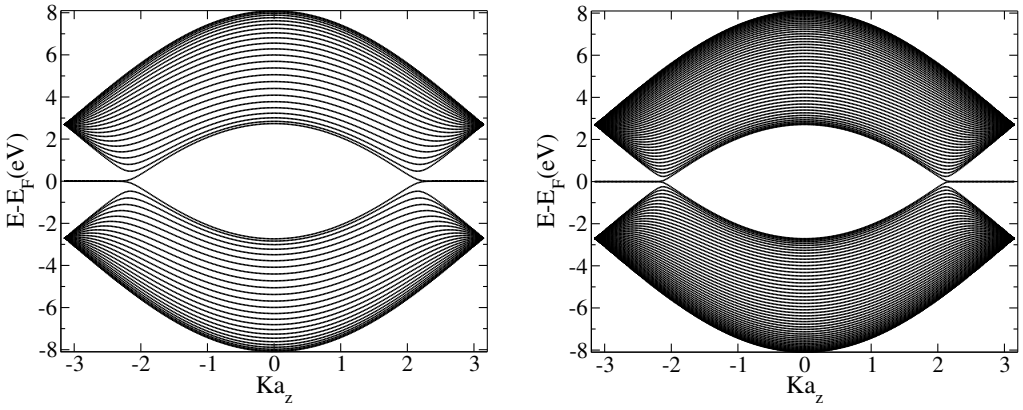

Figure B.1. Energy bands for the graphene electrodes with widths $W = 25$ (left) and 50 (right) C–C bond lengths.

direction; hence the DNA strands are connected to an armchair edge (perpendicular to the zigzag direction) of width W. The thinnest nanoribbons considered are $W = 50$ wide, in units of C–C bond length of 0.142 nm. Bearing in mind that DNA chains exist in many different conformations that on average measure between 2.2 and 2.6 nm in width, the connection of an increasing number of telomeric DNA double strands leads to the use of contacts, up to $W = 500$, in units of C–C bond lengths, in the case of ten telomeric DNA strands in parallel. Figure B.1 shows the energy bands of graphene nanorribons along the zigzag direction for two different widths, $W = 25$ and 50. As can be seen here, from the electronic properties point of view, zigzag-like nanoribbons are metallic with the valence and conduction bands touching at two points as expected (armchair edged nanoribbons may be semiconductor or metallic, depending on the width) [41, 42]. The flat bands at the Fermi energy are localized states at the semi-infinite zigzag edges, giving rise to the peak in the DOS at $E = E_F$ in the inset of figure 5, but showing no influence on the transport properties of the contacted DNA strands. Note also that we have obtained qualitatively similar results—in terms of differences between telomeres and λ- and p53-DNA as well as the lengths dependence of current magnitudes and the robustness of current steps—when using simple square lattice contacts.

References

[1] Fink H-W and Schönenberger C 1999 Electrical conduction through DNA molecules *Nature* **398** 407–10
[2] Porath D, Bezryadin A, Vries S and Dekker C 2000 Direct measurement of electrical transport through DNA molecules *Nature* **403** 635–8
[3] Genereux J C and Barton J K 2010 Mechanisms for DNA charge transport *Chem. Rev.* **110** 1642–62
[4] Feldman A K, Steigerwald M L, Guo X and Nuckolls C 2008 Molecular electronic devices based on single-walled carbon nanotube electrodes *Acc. Chem. Res.* **41** 1731–41
[5] Guo X, Gorodetsky A A, Hone J, Barton J K and Nuckolls C 2008 Conductivity of a single DNA duplex bridging a carbon nanotube gap *Nature Nanotechnol.* **3** 163
[6] Slinker J D, Muren N B, Renfrew S E and Barton J K 2011 DNA charge transport over 34 nm *Nature Chem.* **3** 228–33
[7] Alberts B, Bray D, Lewis J, Raff M, Roberts K and Watson J 1994 *Molecular Biology of the Cell* (New York: Garland)

[8] Leonard F and Talin A A 2011 Electrical contacts to one- and two-dimensional nanomaterials *Nature Nanotechnol.* **6** 773–83
[9] Prins F, Barreiro A, Ruitenberg J W, Seldenthuis J S, Aliaga-Alcalde N, Vandersypen L M K and van der Zant H S J 2011 Room-temperature gating of molecular junctions using few-layer graphene nanogap electrodes *Nano Lett.* **11** 4607–11
[10] Standley B, Bao W, Zhang H, Bruck J, Lau C N and Bockrath M 2008 Graphene-based atomic-scale switches *Nano Lett.* **8** 3345–9
[11] Datta S 1999 *Electronic Transport in Mesoscopic Systems* (Cambridge: Cambridge University Press)
[12] Ferry D K and Goodnick S M 1997 *Transport in Nanostructures* (Cambridge: Cambridge University Press)
[13] Cuniberti G, Macia E, Rodriguez A and Römer R A 2007 Tight-binding modeling of charge migration in DNA devices *Charge Migration in DNA: Perspectives from Physics, Chemistry and Biology* ed T Chakraborty (Berlin: Springer) pp 1–21
[14] Li X-Q and Yan Y J 2001 Electrical transport through individual DNA molecules *Appl. Phys. Lett.* **79** 2190–2
[15] Joe Y S, Lee S H and Hedin E R 2010 Electron transport through asymmetric DNA molecules *Phys. Lett.* A **374** 2367–73
[16] Carvalho R C P, Lyra M L, de Moura F A B F and Domínguez-Adame F 2011 Localization on a two-channel model with cross-correlated disorder *J. Phys.: Condens. Matter* **23** 175304
[17] Klotsa D K, Römer R A and Turner M S 2005 Electronic transport in DNA *Biophys. J.* **89** 2187–98
[18] Wells S A, Shih C-T and Römer R A 2009 Modelling charge transport in DNA using transfer matrices with diagonal terms *Int. J. Mod. Phys.* B **23** 4138–49
[19] Bixon M and Jortner J 2001 Charge transport in DNA via thermally induced hopping *J. Am. Chem. Soc.* **123** 12556–67
[20] Kubař T and Elstner M 2010 Coarse-grained time-dependent density functional simulation of charge transfer in complex systems: application to hole transfer in dna *J. Phys. Chem.* B **114** 11221–40
[21] Cuniberti G, Craco L, Porath D and Dekker C 2002 Backbone-induced semiconducting behavior in short DNA wires *Phys. Rev.* B **65** 241314–4
[22] Rak J, Voityuk A A, Marquez A and Rösch N 2002 The effect of pyrimidine bases on the hole-transfer coupling in DNA *J. Phys. Chem.* B **106** 7919–26
[23] Chakraborty T (ed) 2007 *Charge Migration in DNA: Perspectives from Physics, Chemistry and Biology* (Berlin: Springer)
[24] Berashevich J A and Chakraborty T 2007 Mutational hot spots in DNA: where biology meets physics *Phys. Can.* **63** 103–7
[25] Shih C-T, Wells S A, Hsu C-L, Cheng Y-Y and Römer R A 2012 The interplay of mutations and electronic properties in disease-related genes *Sci. Rep.* **2** 272
[26] Roche S 2003 Sequence dependent DNA-mediated conduction *Phys. Rev. Lett.* **91** 108101–4
[27] López Sancho M P, López Sancho J M and Rubio J 1985 Highly convergent schemes for the calculation of bulk and surface Green-functions *J. Phys. F: Met. Phys.* **15** 851–8
[28] Larsen N B, Biebuyck H, Delamarche E and Michel B 1997 Order in microcontact printed self-assembled monolayers *J. Am. Chem. Soc.* **119** 3017–26
[29] Burdett J K 1984 From bonds to bands and molecules to solids *Prog. Solid State Chem.* **15** 173–255
[30] Damle P, Rakshit T, Paulsson M and Datta S 2002 Current–voltage characteristics of molecular conductors: two versus three terminal *IEEE Trans. Nanotechnol.* **1** 145–53
[31] Zakian V A 1995 Telomeres: beginning to understand the end *Science* **270** 1601–7
[32] Fogg P C M, Allison H E, Saunders J R and McCarthy A J 2010 Bacteriophage lambda: a paradigm revisited *J. Virol.* **84** 6876–9
[33] de Pablo P J, Moreno-Herrero F, Colchero J, Gómez Herrero J, Herrero P, Baró A M, Ordejón P, Soler J M and Artacho E 2000 Absence of DC-conductivity in λ-DNA *Phys. Rev. Lett.* **85** 4992–5
[34] Tran P, Alavi B and Grüner G 2000 Charge transport along the λ-DNA double helix *Phys. Rev. Lett.* **85** 1564–7
[35] Shih C-T, Roche S and Römer R A 2008 Point-mutation effects on charge-transport properties of the tumor-suppressor gene p53 *Phys. Rev. Lett.* **100** 018105

[36] Sherr C J 2004 Principles of tumor suppression *Cell* **116** 235
[37] Tubbs J L and Tainer J A 2011 P53 conformational switching for selectivity may reveal a general solution for specific DNA binding *EMBO J.* **30** 2099–2100
[38] Kitayner M, Rozenberg H, Rohs R, Suad O, Rabinovich D, Honig B and Shakked Z 2010 Diversity in DNA recognition by p53 revealed by crystal structures with Hoogsteen base pairs *Nature Struct. Mol. Biol.* **17** 423–9
[39] Cuniberti G, Craco L, Porath D and Dekker C 2002 Backbone-induced semiconducting behavior in short DNA wires *Phys. Rev.* B **65** 241314
[40] Roy S, Vedala H, Roy A D, Kim D-H, Doud M, Mathee K, Shin H-K, Shimamoto N, Prasad V and Choi W 2008 Direct electrical measurements on single-molecule genomic DNA using single-walled carbon nanotubes *Nano Lett.* **8** 26–30
[41] Castro Neto A H, Guinea F, Peres N M R, Novoselov K S and Geim A K 2009 The electronic properties of graphene *Rev. Mod. Phys.* **81** 109
[42] Nakada K, Fujita M, Dresselhaus G and Dresselhaus M S 1996 Edge state in graphene ribbons: nanometer size effect and edge shape dependence *Phys. Rev.* B **54** 17954–61